Two-nucleon spectral function of the ^{16}O nucleus using the lowest-order constrained variational state-dependent correlation functions of the Reid and Av_{18} interactions

M. Modarres[1,*] and Y. Younesizadeh[2]

[1]*Physics Department, University of Tehran, 1439955961 Tehran, Iran*

[2]*Physics Department, Faculty of Basic Sciences, Tarbiat Modares University of Tehran, Tehran, Iran*

(Received 13 September 2011; revised manuscript received 27 February 2012; published 4 May 2012)

In this work, the two-nucleon spectral functions (TNSFs) are defined in terms of the state- and the density-dependent correlation functions in the framework of the lowest-order constrained variational (LOCV) method to calculate the TNSF of the ^{16}O nucleus in the $^{16}O(e, e'NN)^{14}C$ reaction. The Reid soft-core (Reid68) and the Av_{18} potentials are used as the internucleon interactions. Since, the short-range correlation effects are imposed on the wave functions for the individual channels (e.g., the $^1S_0$ and ^3P_J channels); therefore, the *defect wave functions* are obtained for various channels such that the high relative momenta ($p > 4$ fm^{-1}) are ignored. The resulting TNSFs for the ^{16}O nucleus are compared with those of the dressed random phase approximation (DRPA) calculations of Geurts *et al.* and the experimental predictions, especially those of Onderwater *et al.*, (NIKHEF group), where reasonable agreement is found. It is shown that the optimized state-dependent *defect wave functions* have substantial effects on the TNSF and it is not justified to use the simplified parametrized two-body correlation functions in all of the channels. In agreement with the experimental data of Onderwater *et al.*, the knockout of a $^1S_0$ pair proton dominates the above reaction cross section. Finally, it is demonstrated that the 0^+ and 2^+ peaks, which are expected to be observed in the above reaction cross section, are moved to the lower momenta of out-going protons when the state-dependent correlation functions are imposed.

DOI: 10.1103/PhysRevC.85.054305 PACS number(s): 21.10.Jx, 21.30.Fe, 21.60.−n, 27.20.+n

I. INTRODUCTION

The high-energy inelastic electron scattering experiments from the hadrons and the nuclei, have played a leading role in understanding of the structure of these systems. In particular, the two-nucleon knockout reactions $(e, e'NN)$ are a powerful tool to investigate two-body correlations in nuclei. The $(e, e'NN)$ cross section is related to the two-nucleon spectral functions (TNSFs) which yield the probability to remove two nucleons with momenta $\mathbf{k_1}$ and $\mathbf{k_2}$ from a nucleus, leaving the residual system with the excitation energy ω. So the TNSF contain information on the nuclear structure, the nucleon-nucleon correlations and, in particular, the nucleon-nucleon interactions. One of the features of each nucleus TNSF is the short-range correlations (SRCs) that carry information about nucleon-nucleon correlations and interactions among the constituents of the specific system, which is approximately the same for different nuclei ($\mathcal{A} \geqslant 4$). In contrast to the SRCs, the long-range correlations (LRCs) are sensitive to the whole nuclear system and behave differently when one moves from light nuclei to heavier nuclei. They are related to the low-energy excitations of the nucleus and can be quite different from those in the light nuclei, for which the low-energy excitations are rather sensitive to the shell structure. On the other hand, the nuclear forces indeed are the main factor in the stability of the nucleus, because the LRC and the SRC are much larger than the electrical forces and should be taken into account in calculating any quantity in the above collisions. So one cannot ignore these correlations, even for a very fast probe (i.e., sent to the target), on the assumption that at higher energies the nuclear system can be visualized as a noninteracting Fermi gas.

The spectral function of the many-fermion systems can give us the important quantities of interests; for example, the one-particle ground-state energy, but this may not suffice in the case of three and more nucleon interactions. However, by calculating the TNSF of a nucleus, one can extract the correlation energy between the two particles and finally find the total ground-state energy of the system. Therefore, as was pointed out, the calculation of the TNSF of a nucleus is an important quantity of interest. In recent years, quite a number of theoretical works have been implemented for calculating the two-proton spectral functions with different approximations [1–8]. In these calculations the SRC and the LRC effects have been taken into account by using the different approximations, which have been able to closely explain the experimental properties of the target ground state [1–4]. Barbieri *et al.* has also considered the $^{16}O(e, e'np)$ reaction with the inclusion of the Δ isobar current. The LRCs, which describe the collective motion of nucleons at low energy, were calculated by this group within a model space by solving the hole-hole (hh) DRPA equations.

Obviously, as was mentioned before, the nucleon-nucleon correlations has a major role in the $(e, e'NN)$ reactions than the $(e, e'N)$ reactions. The description of these reactions have been implemented by the Pavia group [9–13]. The abundant experimental results have been also obtained until one can estimate short-range and long-range correlations for the different distances [8,14,15]. In one of the experimental studies, it is shown that the $^1S_0$ proton-pair emission in the $^{16}O(e, e'pp)^{14}C$ reaction is more dominant than the other proton-pair relative states [8,14,15].

*Corresponding author: mmodares@ut.ac.ir

The aim of the present work is to calculate the TNSF of the ^{16}O nucleus in the framework of the lowest-order constrained variational (LOCV) formalism, which is capable of producing the optimized state and the density dependent correlation functions. The validity of the LOCV method, as well as its application to nuclear matter and finite nuclei, has been fully discussed in the works of Owens *et al*. [16–18] and Modarres *et al*. [19–24].

So, the article goes as follows: Section II is started by introducing the fundamental definition of the TNSF and writing down these functions for nucleons with high momentum. We have already studied the one-nucleon-removal spectral function in the impulse approximation (IA) [25–27]. In the IA, two assumptions are mainly made: (1) at high momentum transfer, the target is seen as a set of discrete particles, and (2) the final-state interactions (FSIs) which take place between the hit constituent and the $(\mathcal{A}-1)$-particle spectator system are assumed to be negligible [25]. But in the case of the TNSF, one should focus mainly on the two-nucleon correlations and, for example, the shell structures in the specific nucleus. Therefore, in Sec. III, the short- and long-range correlations are considered by using (i) the LOCV correlation functions, (ii) the two-nucleon interactions, and (iii) the appropriate model space for our single-particle shell structure with inclusion of the wave functions of individual nucleons in the harmonic oscillator basis. The *correlated*, *uncorrelated*, and *defect wave functions* in terms of the different channel correlation functions are also defined. Finally, in the last section, (IV), the numerical results of the two-proton spectral functions and the corresponding ^{16}O$(e,e'NN)^{14}$C cross section are discussed by using the Reid soft-core [28] (Reid68) and Av$_{18}$ [29] interactions and comparing the final-state energies of ^{14}C nucleus with the experimental results to analyze the preciseness of the LOCV approximation against the other theoretical approaches such as the DRPA [1–3,5] as well as the experimental data [8,14,15].

II. CALCULATION OF TNSF OF MANY-FERMION SYSTEMS

The TNSF of many-fermion systems are usually written as

$$\mathcal{S}^{hh}(\mathbf{p}_1,\mathbf{p}_2,,\mathbf{p}'_1,\mathbf{p}'_2,\omega)=\frac{1}{\pi}\mathrm{Im}\mathcal{G}^{hh}(\mathbf{p}_1,\mathbf{p}_2,,\mathbf{p}'_1,\mathbf{p}'_2,\omega), \tag{1}$$

where, in the upper complex plane, the two-particle Green function [30] $\mathcal{G}^{hh}$ is simply defined by

$$\mathcal{G}^{hh}(\mathbf{p}_1,\mathbf{p}_2,,\mathbf{p}'_1,\mathbf{p}'_2,\omega)=\langle 0|a^\dagger_{\mathbf{p}'_1}a^\dagger_{\mathbf{p}'_2}\frac{1}{\mathcal{H}-\mathcal{E}_0+\omega-i\eta}a_{\mathbf{p}_2}a_{\mathbf{p}_1}|0\rangle. \tag{2}$$

Now, if one substitutes equation (2) into equation (1), it is found that

$$\mathcal{S}^{hh}(\mathbf{p}_1,\mathbf{p}_2,,\mathbf{p}'_1,\mathbf{p}'_2,\omega)=\langle 0|a^\dagger_{\mathbf{p}'_1}a^\dagger_{\mathbf{p}'_2}\delta(\omega+\mathcal{H}-\mathcal{E}_0)a_{\mathbf{p}_2}a_{\mathbf{p}_1}|0\rangle. \tag{3}$$

In the above equation $\mathcal{H}$, $|0\rangle$, $(\psi^{\mathcal{A}}_0)$, $\mathcal{E}_0$, and ω are the total Hamiltonian, the ground state, the ground-state energy, and the excitation energy of the target system, respectively. One can simplify equation (3) by using the orthogonality relation (i.e., $\sum_n|n\rangle\langle n|=1$). Therefore, we have

$$\begin{aligned}\mathcal{S}^{hh}&(\mathbf{p}_1,\mathbf{p}_2,,\mathbf{p}'_1,\mathbf{p}'_2,\omega)\\&=\sum_n\langle\psi^{\mathcal{A}}_0|a^\dagger_{\mathbf{p}'_1}a^\dagger_{\mathbf{p}'_2}|\psi^{n,\mathcal{A}-2}\rangle\langle\psi^{n,\mathcal{A}-2}|a_{\mathbf{p}_2}a_{\mathbf{p}_1}|\psi^{\mathcal{A}}_0\rangle\\&\quad\times\delta\big(\omega-(\mathcal{E}^{0,\mathcal{A}}-\mathcal{E}^{n,\mathcal{A}-2})\big),\end{aligned} \tag{4}$$

where, as we stated before, $\psi^{\mathcal{A}}_0$ is the target ground state (in this work the ^{16}O nucleus), and $\psi^{n,\mathcal{A}-2}$ denotes the nth excited state of the residual nucleus (in this work the ^{14}C nucleus). $a^\dagger_{\mathbf{p}}$ $(a_{\mathbf{p}})$ are the creation (destruction) operators of nucleons with momentum $\mathbf{p}$. Now we can expand the creation (destruction) operators in terms of the shell-model quantum numbers to write the TNSF in terms of the final states with angular momentum $\mathcal{J}$. Therefore, it is assumed that

$$a_{\mathbf{p}}=a|p\rangle=\sum_\eta a|\eta\rangle\langle\eta|p\rangle=\sum_\eta\phi_\eta(\mathbf{p})\mathbf{a}_\eta, \tag{5}$$

where $\eta=\{n_\eta,l_\eta,j_\eta,m_\eta\}$. The pair wave function of the creation (destruction) particles in the angular momentum coupled form of $\mathcal{J}$ and M is written as [30–32]

$$\Phi^{\mathcal{J}M}_{ab}(\mathbf{p}'_1,\mathbf{p}'_2)=\sum_{m_\gamma m_\delta}(j_\gamma m_\gamma j_\delta m_\delta|\mathcal{J}M)\phi_\gamma(\mathbf{p}'_1)\phi_\delta(\mathbf{p}'_2). \tag{6}$$

In the above equation, the Clebsch-Gordan coefficient is employed and the indices a and b denote the basis states without the magnetic quantum number (m_a) (i.e., $a=\{n_a,l_a,j_a\}$). Then, it is possible to write equation (4) in terms of the angular momentum $\mathcal{J}$ and simplify the resulting equation by using equations (5) and (6):

$$\begin{aligned}S^{hh}_{\mathcal{J}}&(\mathbf{p}_1,\mathbf{p}_2,,\mathbf{p}'_1,\mathbf{p}'_2,\omega)\\&=\sum_{n,M}\langle\psi^{\mathcal{A}}_0|(a^\dagger_{\mathbf{p}'_1}a^\dagger_{\mathbf{p}'_2})_{\mathcal{J}M}|\psi^{n,\mathcal{A}-2}\rangle\langle\psi^{n,\mathcal{A}-2}|(a_{\mathbf{p}_2}a_{\mathbf{p}_1})_{\mathcal{J}M}|\psi^{\mathcal{A}}_0\rangle\\&\quad\times\delta\big(\omega-(\mathcal{E}^{0,\mathcal{A}}-\mathcal{E}^{n,\mathcal{A}-2})\big),\end{aligned} \tag{7}$$

where

$$\begin{aligned}(a^\dagger_{\mathbf{p}'_1}a^\dagger_{\mathbf{p}'_2})_{\mathcal{J}M}&=\sum_{ab}\Phi^{\star JM}_{ab}(\mathbf{p}'_1,\mathbf{p}'_2)(a^\dagger_a a^\dagger_b)_{\mathcal{J}M},\\(a_{\mathbf{p}_1}a_{\mathbf{p}_2})_{\mathcal{J}M}&=\sum_{cd}\Phi^{\mathcal{J}M}_{cd}(\mathbf{p_1},\mathbf{p_2})(a_c a_d)_{\mathcal{J}M}.\end{aligned} \tag{8}$$

The TNSF can be evaluated in terms of the coupled wave function and the two-nucleon-removal amplitude $(X^{n\star}_{abJ})$ (also see Table I and the related discussion in the Sec. IV):

$$\begin{aligned}S^{hh}_{\mathcal{J}}&(\mathbf{p}_1,\mathbf{p}_2,,\mathbf{p}'_1,\mathbf{p}'_2,\omega)\\&=\sum_n\sum_{abcd,M}\Phi^{\star\mathcal{J}M}_{ab}(\mathbf{p}'_1,\mathbf{p}'_2)X^{n\star}_{abJ}X^{n}_{cd\mathcal{J}}\Phi^{\mathcal{J}M}_{cd}(\mathbf{p}_1,\mathbf{p}_2)\\&\quad\times\delta\big(\omega-(\mathcal{E}^{0,\mathcal{A}}-\mathcal{E}^{n,\mathcal{A}-2})\big),\end{aligned} \tag{9}$$

where

$$X^{n\star}_{ab\mathcal{J}}=\langle\psi^{\mathcal{A}}_0||(a^\dagger_a a^\dagger_b)_{\mathcal{J}}||\psi^{n,\mathcal{A}-2}_{\mathcal{J}}\rangle. \tag{10}$$

In above equations, again the completeness relations $\sum_n |\psi_{\mathcal{J}}^{n,\mathcal{A}-2}\rangle\langle\psi_{\mathcal{J}}^{n,\mathcal{A}-2}| = 1$ for the final states (i.e., the ^{14}C nucleus) have been used. Therefore, the different states are orthogonal:

$$\left\langle \psi_{\mathcal{J}}^{n,\mathcal{A}-2} \middle| \psi_{\mathcal{J}'}^{n',\mathcal{A}-2} \right\rangle = \delta_{\mathcal{J}\mathcal{J}'}\delta_{nn'},$$

which topic this point that $(a_c a_d)_{\mathcal{J}M}|\psi_0^{\mathcal{A}}\rangle$ are the superposition of states (e.g., $|\psi_{\mathcal{J}M}^{n,\mathcal{A}-2}\rangle$) as far as $X_{ab\mathcal{J}}^{n}$ are nonzero. This condition decreases the number of statements for the calculation of $S_{\mathcal{J}}^{hh}$.

III. LOCV STATE AND DENSITY-DEPENDENT CORRELATION FUNCTIONS $f_\alpha^{(p)}(r_{12}, \rho)$ AND NUCLEUS WAVE FUNCTION $\psi_0^{\mathcal{A}}$

In order to proceed further, beside the harmonic oscillator wave functions that are used as the single-particle state of the ^{16}O nucleus, the two-body correlation functions in the specific channels (e.g., $^1S_0$, ^3P_J, etc.) are needed. They are taken from our LOCV calculation for the nuclear matter at the given density of the ^{16}O nucleus [see equations (27)–(30), below]. So it is useful to briefly introduce the application of the LOCV formalism to nuclear matter and nuclei.

The nuclear matter Hamiltonian is usually written as

$$\mathcal{H} = \sum_i T_i + \frac{1}{2}\sum_{i\neq j} V_{ij}, \tag{11}$$

where T_i and V_{ij} are the one-body kinetics and the two-body nucleon-nucleon potential operators, respectively. While T_i is $-\hbar^2{\nabla_i}^2/(2m)$, V_{ij} has a complicated structure of the various phenomenological nucleon-nucleon potentials. The Reid soft-core potential (Reid68) [28] has the channel-dependent structure with the following operator dependency:

$$V_{ij} = \sum_{\alpha,k} v_k^\alpha(ij)\mathbf{O}_k, \tag{12}$$

where $\alpha = \{J,\ L,\ S,\ T\}$ (the relative quantum numbers of two nucleons) and $k = 1,\ 2,\ 3$ [note that $v_k^\alpha(ij)$ are channel dependent]. $\mathbf{O}_k$ are operators and are equal to 1, $\mathbf{S}_{12}$ (the noncentral tensor operator for the $NN \to NN$ transition), and $\mathbf{L}\cdot\mathbf{S}$ (the spin-orbit coupling).

On the other hand, the *operator*-type potentials such as the Argonne Av$_{18}$ interaction [29], which is also intended to be used in this work, are usually written as follows:

$$V_{ij} = \sum_k v_k(ij)\mathbf{O}_k(ij), \tag{13}$$

where, respectively,

$$\begin{aligned} &O_{k=1} \text{ to } O_{k=14} \\ &= 1,\ (\boldsymbol{\sigma_1}\cdot\boldsymbol{\sigma_2}),\ (\boldsymbol{\tau_1}\cdot\boldsymbol{\tau_2}),\ (\boldsymbol{\sigma_1}\cdot\boldsymbol{\sigma_2})(\boldsymbol{\tau_1}\cdot\boldsymbol{\tau_2}),\ \mathbf{S}_{12},\ (\boldsymbol{\tau_1}\cdot\boldsymbol{\tau_2})\mathbf{S}_{12}, \\ &\quad\times \mathbf{L}\cdot\mathbf{S},\ (\boldsymbol{\tau_1}\cdot\boldsymbol{\tau_2})\mathbf{L}\cdot\mathbf{S},\ \mathbf{L}^2,\ (\boldsymbol{\tau_1}\cdot\boldsymbol{\tau_2})\mathbf{L}^2,\ (\boldsymbol{\sigma_1}\cdot\boldsymbol{\sigma_2}) \\ &\quad\times \mathbf{L}^2,\ (\boldsymbol{\sigma_1}\cdot\boldsymbol{\sigma_2})(\boldsymbol{\tau_1}\cdot\boldsymbol{\tau_2})\mathbf{L}^2,\ (\mathbf{L}\cdot\mathbf{S})^2,\ (\boldsymbol{\tau_1}\cdot\boldsymbol{\tau_2})(\mathbf{L}\cdot\mathbf{S})^2, \end{aligned} \tag{14}$$

with the four additional operators which break the charge independence in the Av$_{18}$ interaction:

$$\mathbf{O}_{k=15} \text{ to } \mathbf{O}_{k=18} = \mathbf{T}_{12},\ (\boldsymbol{\sigma_1}\cdot\boldsymbol{\sigma_2})\mathbf{T}_{12},\ \mathbf{S}_{12}\mathbf{T}_{12},\ (\tau_{z1}+\tau_{z2}). \tag{15}$$

$\mathbf{T}_{12}$ is the corresponding noncentral isotensor operator. The eighteen components of the above operators, $v_k(r_{12})$ are purely central functions with no additional dependence on the two nucleons' relative quantum numbers (α) [29] [unlike the Reid-type interactions, there is no explicit channel dependency for the functions, $v_p(r_{12})$], and they are labeled $c,\ \sigma,\ \tau,\ \sigma\tau,\ t,\ t\tau,\ ls,\ ls\tau,\ l2,\ l2\sigma,\ l2\tau,\ l2\sigma\tau,\ ls2,\ ls2\tau,\ T,\ \sigma T,\ tT$, and τz.

In the LOCV formalism, we consider a trial many-body wave function of the following form to evaluate the Rayleigh-Ritz upper bound to the ground-state energy [33,34]:

$$\psi_v = \mathcal{F}\Phi, \tag{16}$$

where Φ is a slater determinant of the plane waves of the $\mathcal{A}$ independent nucleons,

$$\Phi = \mathbb{A}\prod_i \exp(i\vec{k}_i\cdot\vec{r}_i). \tag{17}$$

$\mathcal{F}$ is the $\mathcal{A}$-body correlation operators which will be approximated by its Jastrow type [35]; namely,

$$\mathcal{F}(1\cdots\mathcal{A}) = \mathbb{S}\prod_{i>j}\mathcal{F}(ij), \tag{18}$$

and $\mathbb{A}$ and $\mathbb{S}$ are antisymmetrizing and a symmetrizing operators, respectively. The cluster expansion energy is written as [16–24]

$$\mathcal{E}([f]) = \frac{1}{\mathcal{A}}\frac{\langle\psi_v\,|\,H\,|\,\psi_v\rangle}{\langle\psi_v\,|\,\psi_v\rangle} = \mathcal{E}_1 + \mathcal{E}_2 + \mathcal{E}_3 + \cdots \geqslant \mathcal{E}_0, \tag{19}$$

where $\mathcal{E}_0$ is the true ground-state energy of nuclear matter. In the lowest order, the above series are truncated after the two-body cluster term $\mathcal{E}_2$. The one-body term $\mathcal{E}_1$ is just the familiar Fermi gas kinetic energy:

$$\mathcal{E}_1 = \frac{1}{\mathcal{A}}\sum_i T_i = \frac{1}{\mathcal{A}}\sum_i \frac{\hbar^2{k_i}^2}{2m} = \frac{3}{5}\frac{\hbar^2{k_F}^2}{2m}, \tag{20}$$

where $k_F = (\frac{3}{2}\pi^2\rho)^{1/3}$ and ρ are the Fermi momentum and the density of uniform nuclear matter, respectively. The two-body energy $\mathcal{E}_2$ is

$$\mathcal{E}_2 = \frac{1}{2\mathcal{A}}\sum_{ij}\langle ij\,|\,\mathcal{V}(12)\,|\,ij\rangle_a, \tag{21}$$

and the "effective interaction operator" $\mathcal{V}(12)$ [33–35] is

$$\mathcal{V}(12) = -\frac{\hbar^2}{2m}\big[\mathcal{F}(12),\big[\nabla_{12}^2,\mathcal{F}(12)\big]\big] + \mathcal{F}(12)V(12)\mathcal{F}(12). \tag{22}$$

The two-body matrix elements $\langle ij|O|ij\rangle_a$ are antisymmetrized with respect to the single-particle plane waves, and the

two-body correlation operators $\mathcal{F}(ij)$, which depend on the different channels and the density, are defined as [16–24]

$$\mathcal{F}(ij) = \sum_{\alpha,p=1}^{3} f_{\alpha}^{(p)} \mathcal{O}_{\alpha}^{(p)}(ij). \tag{23}$$

Again, $\alpha = \{J,\ L,\ S,\ T\}$ and the operators $\mathcal{O}_{\alpha}^{(p)}(ij)$ are assumed as follows:

$$\mathcal{O}_{\alpha}^{(p)} = 1,\ \mathbf{S}_{12}. \tag{24}$$

The values of p are set to unity for $L = 0$ and the spin-triplet channels with $L \neq J \neq 1$. But for the $L = J \pm 1$ channels, it takes the values of 2 and 3. As in our previous works, it is also required that the correlation functions $f_{\alpha}^{(1)}$, $f_{\alpha}^{(2)}$, and $(f_{\alpha}^{(3)})$ heal to the Pauli function $f_P(r)$ (zero),

$$f_P(r) = \left\{1 - \left[\frac{3}{2} l(k_F r)\right]^2\right\}^{-1/2}, \tag{25}$$

where $J_J(x)$ are the spherical Bessel functions

$$l(x) = \frac{J_1(x)}{x}. \tag{26}$$

Note that, in our previous works [16–24], the coupled tensor channels have been projected to $(\frac{2}{3} + \frac{1}{6} S_{12}^I)$ and $(\frac{1}{3} - \frac{1}{6} S_{12}^I)$ operators in order to have the same boundary condition for all correlation functions. Then, in this format, one finds $f_{\alpha}^{(2)} = [\frac{2}{3} F_{\alpha}^{(2)} + \frac{1}{3} F_{\alpha}^{(3)}]$ and $f_{\alpha}^{(3)} = \frac{1}{6}[F_{\alpha}^{(2)} - F_{\alpha}^{(3)}]$, where $F_{\alpha}^{(2)},\ F_{\alpha}^{(3)} \to f_P(r)$; that is, the same boundary condition as the pure central channels (the shapes of the LOCV state-dependent correlation functions in the various channels are given in the Figs. 4 to 7 of Ref. [36]).

The normalization constraint $\langle \psi_v \mid \psi_v \rangle = 1$ that we impose on the channel two-body correlation functions $f_{\alpha}^{(p)}$, as well as the coupled and the uncoupled differential equations coming from the Euler-Lagrange equations, are described in Refs. [16–24].

Now, the works of Modarres *et al.* [23,24,37,38] are followed to calculate approximately the two-body wave functions and the two-nucleon overlap functions for each channel by using the above density- and state-dependent correlation functions in the harmonic oscillator basis, similar to the dressed random phase approximation (DRPA) of Refs. [1–3]. As usual,

$$\begin{aligned} \mathbf{r} &= \frac{1}{\sqrt{2}}(\mathbf{r_1} - \mathbf{r_2}) = \frac{1}{\sqrt{2}}\mathbf{r_{12}}, \\ \mathbf{R} &= \frac{1}{\sqrt{2}}(\mathbf{r_1} + \mathbf{r_2}) = \sqrt{2}\mathbf{R_{12}}, \end{aligned} \tag{27}$$

are defined and (here again it is assumed that $\{\alpha = L,\ J,\ S,\ T\}$ with abbreviations $[j] = 2j + 1$, etc., and the first and the second curly brackets are the $6 - j$ and the $9 - j$ symbols [31], respectively),

$$\begin{aligned} \psi^{\mathcal{A},\alpha,(p)}(\mathbf{r},\mathbf{R}) = &\sum_{[a,b]\in\mathcal{M}\neq(\alpha,p)} \mathcal{C}_{ab} f_{\alpha}^{(p)}\left(\sqrt{2}r, \rho\left(\frac{R}{\sqrt{2}}\right)\right) \\ &\times \langle \mathbf{r}, \mathbf{R} | \alpha, nL, N\mathcal{L}\rangle, \end{aligned} \tag{28}$$

with [the model space $\mathcal{M}$ is explained after equation (34) and $[a, b]$ means a summation over all of the quantum numbers, except those indicated],

$$\begin{aligned} \mathcal{C}_{ab} = &\frac{1}{\sqrt{2}}\{[j_a][j_b][\mathcal{J}][\lambda]^2[S][J][T](1 - (-1)^{l+S+T})\}^{\frac{1}{2}} \\ &\times \begin{Bmatrix} \mathcal{L} & L & \lambda \\ S & \mathcal{J} & J \end{Bmatrix} \begin{Bmatrix} l_a & \frac{1}{2} & j_a \\ l_b & \frac{1}{2} & j_b \\ \lambda & S & \mathcal{J} \end{Bmatrix} \\ &\times (-1)^{(\mathcal{L}+\lambda+J+S)} \langle n_a l_a, n_b l_b, \lambda \mid nL, N\mathcal{L}, \lambda\rangle, \end{aligned} \tag{29}$$

where the local-density approximation has been used [23,24,37,38]; that is, $\frac{1}{2}[\rho(|\mathbf{r_1}|) + \rho(|\mathbf{r_2}|)]$ is replaced by $\rho(|\frac{\mathbf{R}}{\sqrt{2}}|) = \rho(\frac{|\mathbf{r_1}+\mathbf{r_2}|}{2})$. $\langle n_a l_a, n_b l_b, \lambda | nL, N\mathcal{L}, \lambda\rangle$ are the familiar Brody-Moshinsky brackets [39] and a and b run over the occupied orbits in the independent-particle model. In the above equations, the uncorrelated one-body density is defined as follows in terms of the harmonic oscillator wave functions for each nucleus:

$$\rho(\mathbf{r_j}) = \sum_{i}^{\mathcal{A}} |\langle \mathbf{r_j} | i, \hbar\omega\rangle|^2. \tag{30}$$

$\psi_0^{\mathcal{A}}(\mathbf{r}, \mathbf{R})$ can be calculated for given $\mathcal{A}$ by summing over α and p in equation (28). However, in this work, the complexity of the center-of-mass dependence of the correlation functions is ignored and the input correlation functions for each channel is used at the empirical nuclear matter density (i.e., 0.17 fm^{-3}) with the corresponding channel energy (this approximation will be investigated in future works). So, with this assumption, equation (28) reads

$$\begin{aligned} &\psi^{A,\alpha,p}(\mathbf{r},\mathbf{R}) \\ &\quad = \sum_{a,b} \mathcal{C}_{ab} f_{\alpha}^{p}(\sqrt{2}r, \rho = 0.17)\langle \mathbf{r}, \mathbf{R} | \alpha, nL, N\mathcal{L}\rangle, \end{aligned} \tag{31}$$

which can be simply separated into the relative and the center-of-mass coordinate,

$$\begin{aligned} &\psi^{A,\alpha,p}(\mathbf{r},\mathbf{R}) \\ &\quad = \sum_{a,b} \mathcal{C}_{ab}\left[f_{\alpha}^{p}(\sqrt{2}r, \rho = 0.17)\langle \mathbf{r} | \alpha, nL\rangle\right][\langle \mathbf{R} | N\mathcal{L}\rangle]. \end{aligned} \tag{32}$$

The radial part of the above equation in the different channels and in terms of our channel-, tensor-, and density-dependent correlation functions, which will be used to calculate the *defect function* [1,2], can be written as follows:

$$\begin{aligned} \psi(^1S_0) &= f_{^1S_0}^{(1)} \phi(^1S_0), \\ \psi(^3P_0) &= f_{^3P_0}^{(1)} \phi(^3P_0), \\ \psi(^3P_1) &= f_{^3P_1}^{(1)} \phi(^3P_1), \\ \psi(^3P_2) &= \left[f_{^3P_2 - {}^3F_2}^{(1)} - \tfrac{2}{5} f_{^3P_2 - {}^3F_2}^{(2)}\right]\phi(^3P_2) \\ &\quad + 6\sqrt{6} f_{^3P_2 - {}^3F_2}^{(2)} \phi(^3F_2), \\ \psi(^1D_2) &= f_{^1D_2}^{(1)} \phi(^1D_2), \\ \psi(^3F_2) &= \left[f_{^3P_2 - {}^3F_2}^{(1)} - \tfrac{8}{5} f_{^3P_2 - {}^3F_2}^{(2)}\right]\phi(^3F_2) \\ &\quad + 6\sqrt{6} f_{^3P_2 - {}^3F_2}^{(2)} \phi(^3P_2), \end{aligned} \tag{33}$$

where the quantities ϕ are the relative parts of the two-nucleon harmonic oscillator wave functions in the related channel. Obviously, the Fourier transform of equations (32) or (33) can be used to calculate $\psi^{A,\alpha,p}(\mathbf{p},\mathbf{P})$ or $\psi^{A,\alpha,p}(\mathbf{p})$ by ignoring the center-of-mass dependence.

In order to calculate the TNSF for the ^{16}O$(e,e'pp)^{14}$C reaction:

$$\mathcal{S}^{hh}_{\mathcal{J}}(\mathbf{p}_1,\mathbf{p}_2,,\mathbf{p'}_1,\mathbf{p'}_2,\omega) = \sum_n \sum_{[abcd]\in\mathcal{M}\neq\mathcal{J},M} \Psi^{\star\mathcal{J}M}_{ab}(\mathbf{p'}_1,\mathbf{p'}_2) X^{n\star}_{ab\mathcal{J}} X^{n}_{cd\mathcal{J}} \Psi^{\mathcal{J}M}_{cd} \times(\mathbf{p}_1,\mathbf{p}_2)\delta\big(\omega-\mathcal{E}^{n,\mathcal{A}-2}_{\mathcal{J}}\big), \quad (34)$$

in which the uncorrelated shell-model wave functions $\Phi^{\mathcal{J}M}_{cd}(\mathbf{p}_1,\mathbf{p}_2)$ have been replaced by the correlated ones [i.e., $\Psi^{\mathcal{J}M}_{cd}(\mathbf{p}_1,\mathbf{p}_2)$]. So, one should calculate $\Psi^{\mathcal{J}M}_{ab}(\mathbf{p}_1,\mathbf{p}_2)$ and $X^{n}_{ab\mathcal{J}}$ [see equations (6) and (10), respectively] in the center of mass and the relative coordinate in momentum space. This can be done by using equations (23), (28), and (29). The ^{16}O and ^{14}C nucleus wave functions, which are needed in equation (10), are defined as

$$\psi^{\mathcal{A}=16}_{0}(\mathbf{r},\mathbf{R}) = \sum_{\alpha,p} \psi^{\mathcal{A}=16,\alpha,(p)}(\mathbf{r},\mathbf{R}), \quad (35)$$

and

$$\psi^{n,\mathcal{A}=14}_{\mathcal{J}}(\mathbf{r},\mathbf{R}) = \sum_{[a,b]\in\mathcal{M}\neq\mathcal{J}} \mathcal{C}_{ab} f^{(p)}_{\alpha}\left(\sqrt{2}r,\rho\left(\frac{R}{\sqrt{2}}\right)\right) \times\langle\mathbf{r},\mathbf{R}|\alpha,nL,N\mathcal{L}\rangle, \quad (36)$$

respectively. For calculation of $\Psi^{\mathcal{J}M}_{cd}(\mathbf{p}_1,\mathbf{p}_2)$ the following equation is used:

$$\Psi^{\mathcal{J}M}_{ab}(\mathbf{p}_1,\mathbf{p}_2) = [\mathcal{F}(|\mathbf{p}_1-\mathbf{p}_2|)]_{\mathcal{J}=\mathbf{J}+\mathbf{L}+\mathbf{S}}\,\Phi^{\mathcal{J}M}_{ab}(\mathbf{p}_1,\mathbf{p}_2). \quad (37)$$

Then, by inserting the equations (35) and (36) in equation (10) and using the Wigner-Eckart theorem for the reduced second-rank tensor [31], the matrix elements in question (i.e., the shell model amplitudes) can be evaluated. Note that, in the above equations, the summation over the shell-model configurations has also been limited to the model space $\mathcal{M}$ which is discussed in Refs. [1–3]. So, in this work, the SRC and the LRC are considered in the LOCV approximation, but with a similar procedure as that of Refs. [1–3], which will be discussed below. In Refs. [1–3], the Bethe-Goldstone equation (BGE) has been used for consideration of both the SRC and the LRC. In these references, the SRC has also been discussed in the framework of the correlated basis function (CBF) method [40]. However, in the CBF formalism, the correlated many-body wave functions are not fully state dependent and usually are simply parametrized [1–3,40–43]. In the present paper, the model space $\mathcal{M}$ is also limited to the $1s$ up to the $2p$ $1f$ harmonic oscillator shell-model configuration (rather than the $1s$ and the $1p$ shells, but up to the large $100\hbar\omega$ in the harmonic oscillator basis) in the ^{16}O nucleus. With these assumptions, as was discussed in the introduction, the SRC and the LRC are treated independently within the correlation functions $f^{(p)}_{\alpha}$ and the shell-model amplitude $X^{n}_{cd\mathcal{J}}$, respectively, with the limited space $\mathcal{M}$ [1–4].

Finally, analogous to the BGE, from equation (28), the *total defect wave functions* can be written as [also see equation (33)]

$$\chi^{\alpha}(\mathbf{r},\mathbf{R}) = \sum_{[a,b]\in\mathcal{M}\neq\alpha} \mathcal{C}_{ab}\left[f^{p}_{\alpha}\left(\sqrt{2}r,\rho\left(\frac{R}{\sqrt{2}}\right)\right)-1\right] \times\langle\mathbf{r},\mathbf{R}|\alpha,nL,N\mathcal{L}\rangle, \quad (38)$$

and with the omission of this center-of-mass dependence of the correlation functions [see equation (32)],

$$\chi^{\alpha}(\mathbf{r},\mathbf{R}) = \sum_{[a,b]\in\mathcal{M}\neq\alpha} \mathcal{C}_{ab}\big[f^{p}_{\alpha}(\sqrt{2}r,\rho=0.17)-1\big] \times\langle\mathbf{r}|\alpha,nL\rangle\langle\mathbf{R}|N\mathcal{L}\rangle, \quad (39)$$

where, similar to Ref. [3], the Fourier transform of the relative part of equation (39), $\chi^{\alpha}(r)$, can be used to calculate the *defect wave functions*, $\chi^{\alpha}(\mathbf{p})$. For example:

$$\chi^{^1S_0}(r) = R_{00}(r)\big[f^{(1)}_{^1S_0}(\rho=0.17,r)-1\big], \quad (40)$$

in which $R_{00}(r)$ is the relative part, with $n=0,\quad L=0$, of the two-nucleon harmonic oscillator wave function, etc. As was pointed out before, the shape of our state- and density-dependent correlation functions has been given in Ref. [36]. But it is clearly seen from equation (38) that, in general, it is not possible to factorize the calculated *defect function* for the finite nuclei into the product of wave functions depending on the relative and center-of-mass coordinate [1] [see discussion after equation (33) of this reference], unless one averages over the center-of-mass coordinate. But here our correlation functions are state dependent and the different states are orthogonal to each other. On the other hand, because of the LOCV normalization constraint, which comes from the convergence of the cluster expansion [22,34],

$$\langle\Psi\mid\Psi\rangle = 1+\kappa_2+\kappa_3+\cdots, \quad (41)$$

and the overshot behavior of the LOCV correlation functions, we have $\kappa_2=0$ and $\kappa_3\leqslant 10^{-3}$. So in the LOCV framework, even the normalization of the total wave function is satisfied (see Refs. [23,24]).

As was stated in the introduction and in the above equations, both the short- and the long-range parts of the nucleon correlations have been employed (i.e., the SRC) via the state- and the density-dependent correlation functions from our LOCV calculation with the inclusion of nucleon-nucleon interactions and the LRC by the long-range parts of the correlation functions (note that our correlation functions satisfy the Pauli functions, so they do not become unity in the short distances) and the harmonic oscillator configuration space of the removal pair (i.e., the shell structure and the removal energy). Finally, equation (34) can be transformed to the relative and the center-of-mass momentum coordinates of the pair particle with the similar relation as the one used for coordinate space in equation (27):

$$\mathcal{S}^{hh}_{\mathcal{J}}(\mathbf{p},\mathbf{P},,\mathbf{p}',\mathbf{P}',\omega) = \sum_n \sum_{[abcd]\in\mathcal{M}\neq\mathcal{J},M} \Psi^{\star JM}_{ab}(\mathbf{p}',\mathbf{P}') X^{n\star}_{abJ} X^{n}_{cdJ} \Psi^{JM}_{cd}(\mathbf{p},\mathbf{P}) \times\delta\big(\omega-\mathcal{E}^{n,\mathcal{A}-2}_{J}\big). \quad (42)$$

We use the same harmonic oscillator parameters, the configurations, the transformation, etc., which have been adapted in Refs. [1–3,44] for the calculation of the TNSF of the ^{16}O nucleus (see the next section for the numeric values of our LOCV two-nucleon removal amplitudes).

IV. RESULTS, DISCUSSION, AND CONCLUSION

In Fig. 1, the *defect wave functions*, which are the Fourier transform of the radial part of equation (39), are plotted by using our calculated LOCV correlation functions [36] in the different channels for two potentials: the Av$_{18}$ and the Reid68. There is not much difference between the *defect wave functions* of Av$_{18}$ and Reid68 interactions, especially in the $^1S_0$ and the $^3P_1$ channels. A very similar momentum dependence is also observed for the above *defect wave functions* in the other channels. The diamonds are the results of BGE-DRPA [1,2] calculation with the Reid68 potential. There is reasonable agreement between the LOCV and the BGE-DRPA *defect wave functions*. Geurts *et al*. have also compared their BGE-DRPA *defect wave functions* with those of CBF [1–3,40–43] (the filled diamonds), but with the Av$_{14}$ interaction. Similar discrepancies are also observed between the BGE-DRPA and the CBF results. Since there is not much difference between the Av$_{14}$ and Av$_{18}$ interactions, one can conclude that our *defect functions* are much closer to those of BGE-DRPA than the CBF, since, as we stated before, in the CBF calculation the correlation functions are not fully state dependent but are simply parametrized (i.e., they are not functionally optimized).

Our LOCV two-proton-removal amplitudes from the ^{16}O nucleus to the ^{14}C nucleus ground state 0^+ are given in Table I. There is not much difference between the amplitudes calculated by us and those given in Table I of Ref. [3]. Similar to the above conclusion, the present result shows that the harmonic oscillator wave functions for each configuration have the main effect on the calculation of the two-proton-removal amplitudes.

The calculated TNSF, equation (42), for the removal of a $^1S_0$ proton pair from the ^{16}O nucleus in terms of the energy ω to the final state in the ^{14}C nucleus, relative to the ground-state energy of the nucleus ^{16}O, are plotted in Fig. 2 by using the Reid68 potential. Note that the first 0^+ state only comes from the two-proton separation energy. In the above figure the excited energy is calculated from $\mathcal{E}_k = \mathcal{T} + \mathcal{E}_2^\alpha$ [16–22], where $\mathcal{T} = (2n + L + 2N + \mathcal{L} + 3)\hbar\omega_0$ [23,24,37,38]. Here, $\alpha = {}^1S_0$ and $\omega_0 = 16.3$ MeV [23,24,37,38], which is near to the oscillator parameter that has been used in the DRPA calculations [1,2] (also see Table I and the similar table in Ref. [3] for the choice of a harmonic oscillator configurations). As was pointed out above, there are not many differences between our $X^{n\star}_{ab\mathcal{J}}$ and those of Geurts *et al*. in Ref. [3]. If one considers the 0^+ peak to have zero energy, then this figure shows that the 2^+ peak (the strongest peak) and the $2^+/0^+$ peak have 6.5 and 10.8 MeV energies, respectively, which are closer to the experimental

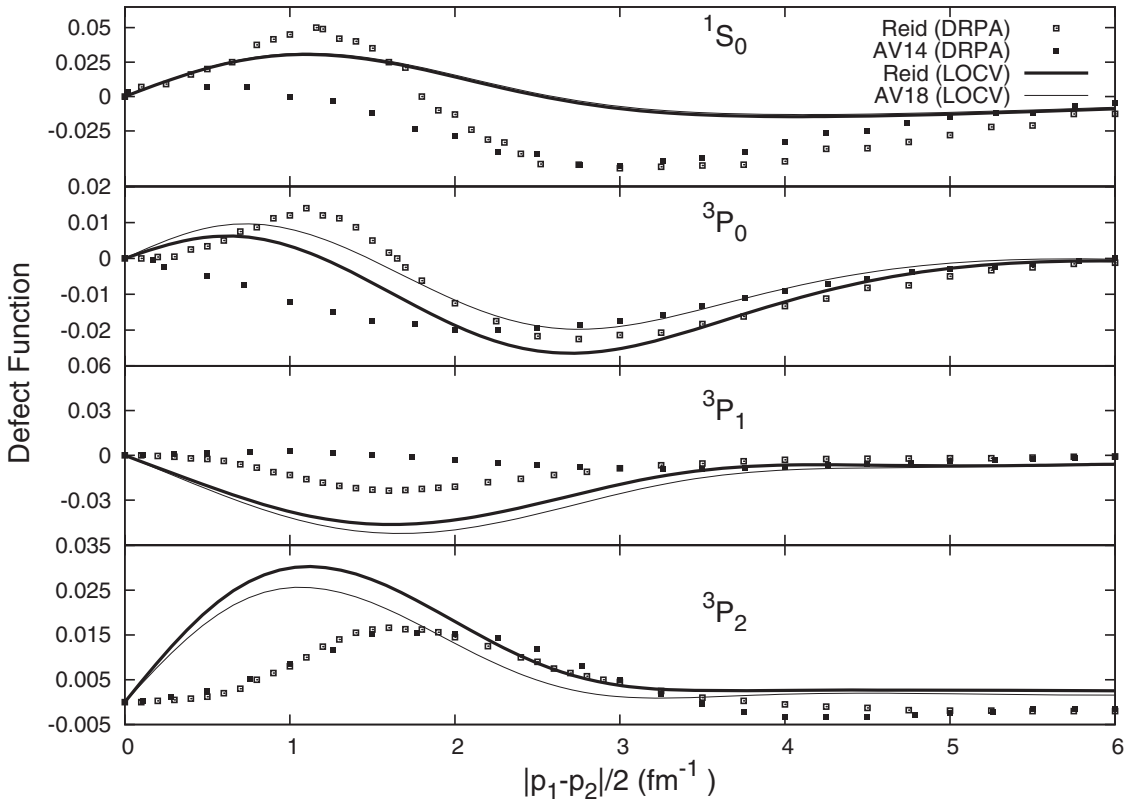

FIG. 1. *Defect wave functions* calculated for different channels with Reid68 (dashed curve) and Av$_{18}$ (full curves) potentials by using LOCV state- and density-dependent correlation functions. The diamonds (filled diamonds) are the BGE-DPRA (CBF) calculations of references [1,2] with the Reid68 (Av$_{14}$) potential.

TABLE I. LOCV two-proton-removal amplitudes $X^{n\star}_{abJ}$ for ^{16}O$(e, e'pp)^{14}$C reaction explained in the text for the model space $0s$ up to $1p0f$. The quantum number ρ is the total number of harmonic oscillator quanta of the pair: $\rho = 2n + L + 2N + \mathcal{L}$.

	n	N	ρ	0^+
$^1S_0; \mathcal{L} = 0$	0	1	2	−0.353
	1	0	2	0.353
	0	0	0	0.088
	1	1	4	−0.069
	0	2	4	0.038
	2	0	4	0.038
	1	2	6	0.023
	2	1	6	−0.023
$^3p_1; \mathcal{L} = 1$	0	0	2	0.610
	0	1	4	+0.030
	1	0	4	−0.030
$^1D_2; \mathcal{L} = 2$	0	0	4	0.023
	n	N	ρ	2^+
$^1S_0; \mathcal{L} = 2$	0	0	2	0.580
	1	0	4	+0.016
	0	1	4	−0.012
$^3p_1; \mathcal{L} = 1$	0	0	2	−0.213
$^3p_2; \mathcal{L} = 1$	0	0	2	−0.362
$^1D_2; \mathcal{L} = 0$	0	0	2	−0.580
	0	1	4	+0.016
	1	0	4	−0.012
	n	N	ρ	1^+
$^3p_0; \mathcal{L} = 1$	0	0	2	+0.526
$^3p_1; \mathcal{L} = 1$	0	0	2	+0.480
$^3p_2; \mathcal{L} = 1$	0	0	2	−0.590

data [1,2,8,14,15,45,46] with respect to those of DRPA. The diamonds show the results of the DRPA of Refs. [1,2] with the same potential. There are overall agreements between the calculated $^1S_0$ TNSF. However, our calculations show that the stronger peak (2^+) exists at higher energies with respect to those of DRPA,. while the second peak appears at the lower energy. We do not find much difference between our calculated TNSF with the Reid68 or Av$_{18}$ interaction. In contrast to Geurts *et al*. [1], the 1^- peak contribution is not spread out, and it has been appeared around 16.1 MeV.

In Fig. 3, the similar calculations as above are performed for the ^3P_J removal of a proton pair of the ^{16}O nucleus for $\mathcal{L} = 0$ (the heavy full curve) and 1 (the light full curve). The results of Geurts *et al*. [1,2] are also given for comparison. There is very good agreement between the LOCV and the DRPA methods in the case of $\mathcal{L} = 1$. But for $\mathcal{L} = 0$, the TNSFs are shifted to higher energy with respect to the DRPA ones. Our 1^+ peak is at 11.5 MeV, which agrees well with the experimental data (i.e., 11.37 MeV [8,14,15,45,46]).

The TNSF for the removal of a $^1D_2$ proton pair by using the Reid68 and Av$_{18}$ potentials are plotted in Fig. 4. In this figure again the ground state 0^+ peak and the strong 2^+ peak exist. As before, there is not much difference between the TNSF calculated with the Reid68 or Av$_{18}$ interaction. It seems that the peaks have shifted to higher energy with the slight changes in the peak maximum. On the other hand, the peaks are as

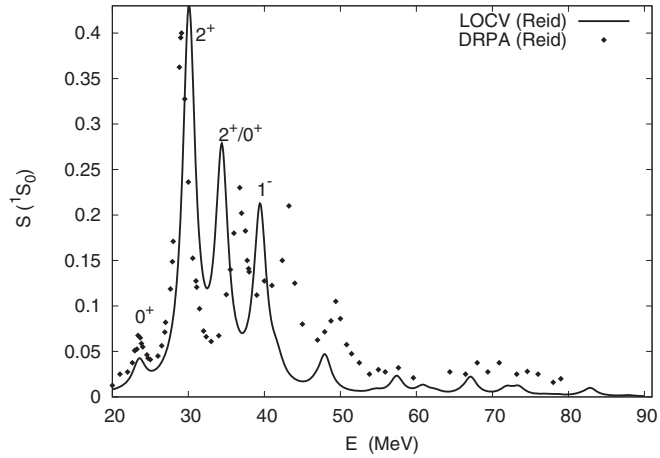

FIG. 2. TNSF equation (42) for the removal of $^1S_0$ proton pair from ^{16}O nucleus in terms of energy ω of final states in ^{14}C nucleus relative to ground-state energy ^{16}O nucleus (with Reid68 interaction). The radial relative quantum number is zero ($n = 0$) and the total angular momentum $\mathcal{L}$ for the center-of-mass coordinates is the same as that of final states. The peaks labeled 0^+, 2^+, $2^+/0^0$, and 1^- are nearly the final states of the ^{14}C nucleus calculated in the LOCV framework. The diamonds are the DRPA of Refs. [1,2] (with the Reid68 interaction).

strong as for the $^1S_0$ case. The $^1D_2$ knockout pair has not been investigated theoretically or experimentally.

The superposition of the spectral functions (SSF) $\hat{\mathcal{S}}(\mathbf{p}'_1, \mathbf{p}'_2, \mathcal{E})$ leads to the removal of two protons with the final momenta $\mathbf{p}'_1$ and $\mathbf{p}'_2$ from the ^{16}O nucleus with the final ^{14}C nucleus at the 0^+ ground state or the first-excited 2^+ state and are plotted in the Figs. 5 to 8 for the Reid68 and Av$_{18}$ interactions. This quantity gives a sensible estimate of the $e + ^{16}\mathrm{O} \to e' + 2p + ^{14}\mathrm{C}$ cross section in which the virtual

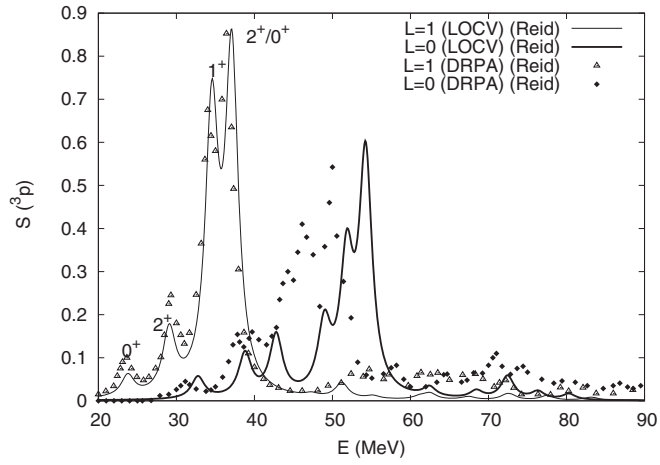

FIG. 3. TNSF for removal of a ^3P_J proton pair in terms of energy ω from ^{16}O nucleus for different center-of-mass angular momenta $\mathcal{L} = 0$ and $\mathcal{L} = 1$ with respect to the final states of ^{14}C nucleus. The peaks labeled 0^+, 2^+,1^+, and $2^+/0^+$ are for $\mathcal{L} = 1$. In these plots, the full and the heavy full curves represent the LOCV calculations with the Reid68 interaction. The diamonds and the triangles are obtained from the DRPA approximations of Refs. [1,2] (again with the Reid68 potential).

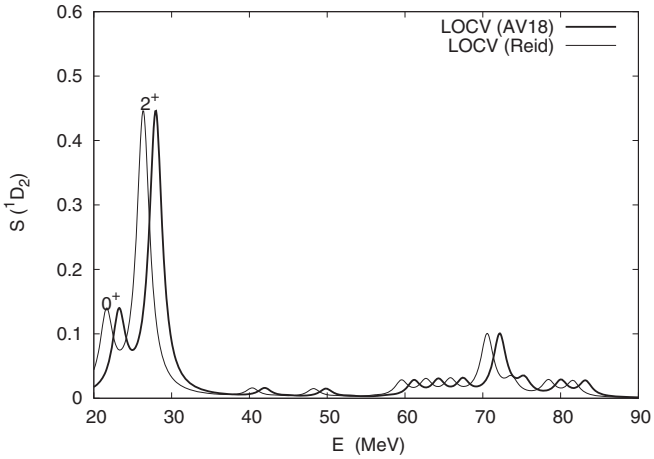

FIG. 4. TNSF for removal of a ${}^1D_2$ proton pair from ^{16}O nucleus by using LOCV formalism. The full curve is for the Reid68 potential and the heavy full curve is for the Av_{18} potential. The peaks point to the probable final states of the ^{14}C nucleus at an energy of about 73.1 MeV and are due to the SRC, which existed in Figs. 2 and 3 as well.

photon with momentum $\mathbf{q}$ is assumed to couple to one of the detected protons. Since the above cross section is proportional to the square of the nuclear charge operator transition matrix element, it becomes equal to the following relation for the corresponding channel α in momentum space [1,2,9]:

$$\begin{aligned}\hat{\mathcal{S}}_\alpha(\mathbf{p}'_1,\mathbf{p}'_2,\mathcal{E}) = {} & \mathcal{S}_\alpha(\mathbf{p}'_1-\mathbf{q},\mathbf{p}'_2,\mathbf{p}'_1-\mathbf{q},\mathbf{p}'_2,\mathcal{E}) \\ & + \mathcal{S}_\alpha(\mathbf{p}'_1-\mathbf{q},\mathbf{p}'_2,\mathbf{p}'_1,\mathbf{p}'_2-\mathbf{q},\mathcal{E}) \\ & + \mathcal{S}_\alpha(\mathbf{p}'_1,\mathbf{p}'_2-\mathbf{q},\mathbf{p}'_1-\mathbf{q},\mathbf{p}'_2,\mathcal{E}) \\ & + S_\alpha(\mathbf{p}'_1,\mathbf{p}'_2-\mathbf{q},\mathbf{p}'_1\mathbf{p}'_2-\mathbf{q},\mathcal{E}). \qquad (43)\end{aligned}$$

Similar to Refs. [1,2], in the above figures, the kinematics and angles of momentum are chosen according to the configuration of the detectors of the proposed measurements (in 1994) at NIKHEF [8,9,14,15,47,48]; that is, the photon momentum $\mathbf{q}$ is fixed along the z axis, with length 313 MeV/c, and the momenta $\mathbf{p}'_1$ and $\mathbf{p}'_2$ are in the same plane with $\mathbf{q}$ at -49

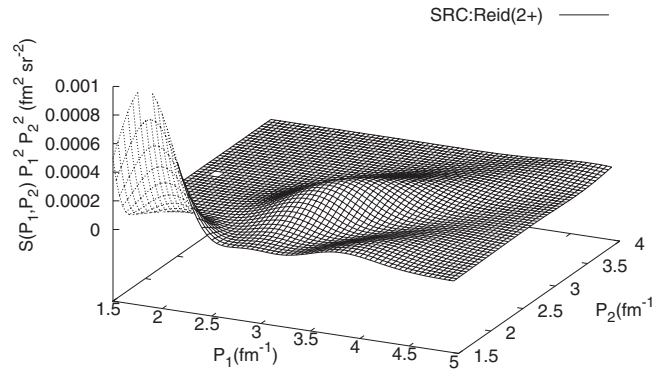

FIG. 6. Superposition of spectral functions $\hat{\mathcal{S}}$ in equation (43), which is suitable for calculation of cross section of ^{16}O$(e,e'pp)^{14}$C reaction. This function is the probability of the removal of two protons with the final momenta $\mathbf{p_1}$ and $\mathbf{p_2}$ leading to the final 0^+ ground state or the first-excited 2^+ state in the ^{14}C nucleus, by using the Reid68 interaction.

and 123 degrees with respect to this transferred momentum $\mathbf{q}$, respectively. Obviously, the delta functions in the spectral functions are removed. Figures 5 and 7 demonstrate the calculated SSF with the Reid68 interaction, which can be compared to the Figs. 9 and 6.8 of Refs. [1] and [2], respectively. Looking at these figures, one can conclude that the inclusion of the LOCV state-dependent correlation functions push $\hat{\mathcal{S}}(\mathbf{p}'_1,\mathbf{p}'_2,\mathcal{E})$ to the lower momenta. On the other hand, our results have better agreement with Fig. 6.9 of the Ref. [2], in which the parametrized state-independent correlation functions are imposed in the DRPA calculation. Now, the interaction is switched from the Reid68 interaction to the Av_{18} potential, and it is clearly seen that the peaks remain approximately in the same place but become much stronger. In general, the peaks are the effect of short-range correlation and should be observed in experiments [8,9,14,15,47,48], as will be discussed later. The plots of omission of SRC are also demonstrated in Figs. 9 and 6.8 of Refs. [1] and [2], respectively, in which, as is expected, the above peaks in the $(\mathbf{p}'_1;\mathbf{p}'_2)$ plane have disappeared. The

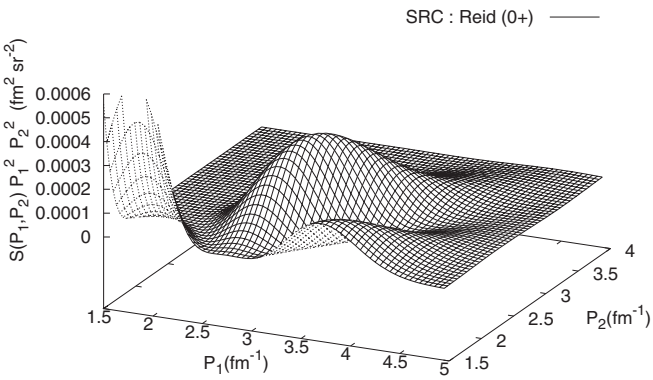

FIG. 5. Superposition of spectral functions $\hat{\mathcal{S}}$ in Eq. (43), which is suitable for calculation of cross section of ^{16}O$(e,e'pp)^{14}$C reaction. This function is the probability of the removal of two protons with the final momenta $\mathbf{p_1}$ and $\mathbf{p_2}$ leading to the final 0^+ ground state or the first-excited 2^+ (see Fig. 6) state in the ^{14}C nucleus, using the Reid68 interaction.

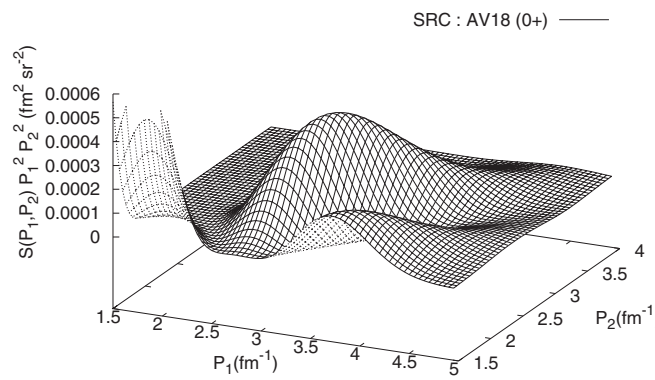

FIG. 7. Superposition of spectral functions $\hat{S}$ in equation (43), which is suitable for calculation of cross section of ^{16}O$(e,e'pp)^{14}$C reaction. This function is the probability of the removal of two protons with the final momenta $\mathbf{P_1}$ and $\mathbf{p_2}$ leading to the final 0^+ ground state or the first-excited 2^+ (see Fig. 8) state in the ^{14}C nucleus, by using the Av_{18} interaction.

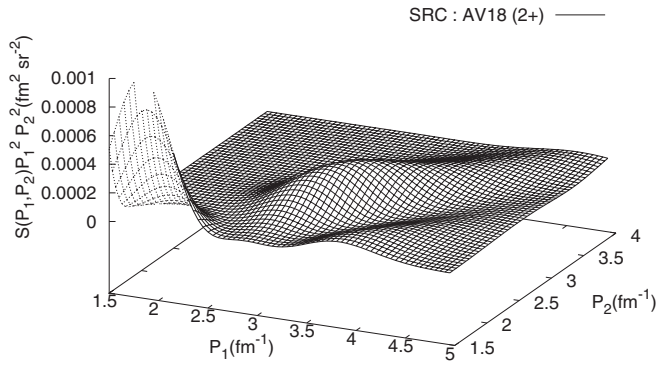

FIG. 8. Spectral function $\hat{S}$ in equation (43), which is suitable for calculation of cross section of ^{16}O$(e, e' pp)^{14}$C reaction. This function is the probability of removal of two protons with the final momenta $\mathbf{P_1}$ and $\mathbf{p_2}$ leading to the final 0^+ ground state or the first-excited 2^+ state in the ^{14}C nucleus (the Av_{18} interaction).

only experimental results which were finally published by the NIKHEF groups are those of Refs. [8,14,15]. The quantities of interest according to these experiments, especially those of Ref. [8], are calculated. In these experiments [8,14,15], the knockout proton detectors subtend the solid angles of 225 and 550 msr and accept protons with energies from 69 to 215 MeV and from 44 to 171 MeV, respectively. The data are taken at an energy transfer $\omega_\gamma = 210$ MeV$/c$ and $|\mathbf{q}| = 300$ MeV and the emission angles of the forward proton with respect to $\mathbf{q}$ are between 20° and 40°. If the missing energies and momenta are defined as $\mathcal{E}_m = \omega_\gamma - T_1 - T_2 - T_{\mathcal{A}-2}$ and $\mathbf{p}_m = \mathbf{q} - \mathbf{p}_1 - \mathbf{p}_2$, respectively, then the excitation energies of the $\mathcal{A}-2$ nucleus (^{14}C) are given by $\mathcal{E}_x = \mathcal{E}_m - S_{NN}$ (S_{NN}). On the other hand, the cross section can be factorized in terms of the TNSF of each channel [8]. In Figs. 9 and 10, $\mathcal{S}_\alpha(p_m, \mathcal{E}_x)$ are plotted according to the above experimental inputs for the $\alpha = {}^1S_0$ and ${}^3P_J$ channels, respectively. In both channels, our LOCV results are in good agreement with Fig. 2 of Ref. [8], especially for the corresponding peaks (i.e., $0^+, 2^+, 2^+/0^+$ and 1^+). However, in the ${}^3P_J$ channels, the peaks are not as strong as for the experimental case (i.e., smaller cross section). Note

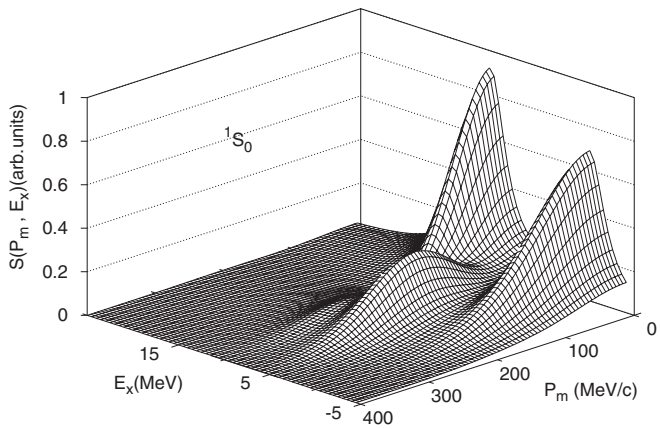

FIG. 9. TNSF $\mathcal{S}(\mathcal{E}_x, p_m)$ for knockout of ${}^1S_0$ pair from $1p$ shell in the ^{16}O nucleus. See text for more explanations.

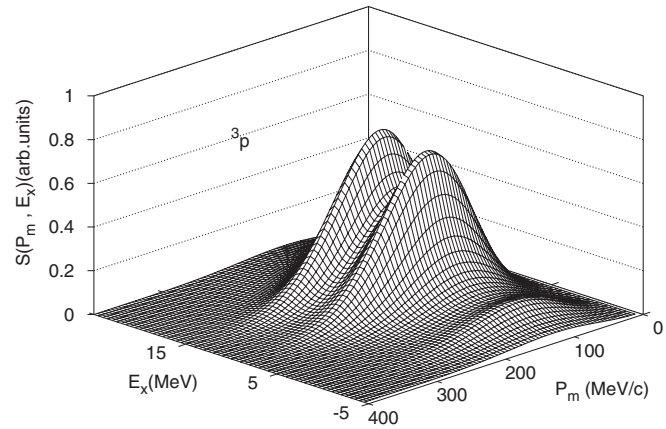

FIG. 10. Same as Fig. 9 but for ${}^3P_J$ channels.

that, in the Ref. [8], the contribution of the ${}^1D_2$ the channel has been ignored.

Finally, in Fig. 11, the similar quantity as above is plotted in terms of the missing momentum, but for different ranges of excitation energies (i.e., $-5 < \mathcal{E}_x < 20$ MeV). This range can be attributed to the emission of predominantly the two-proton knockout ($p < 4$ fm^{-1}). The full and the dash curves are the corresponding parts of ${}^1S_0$ and the ${}^3P_J$, respectively, while the heavy full curves are the total contributions to the cross section. The pluses are the best fit to the corresponding experimental data according to Ref. [8]. Again, an overall agreement with the data for the different range of excitation energies is fined.

In conclusion, the two-nucleon spectral functions of the ^{16}O nucleus are calculated by using the lowest-order constrained variational state-dependent correlation functions with the two inputs interactions; namely, the Reid68 and Av_{18} potentials. The spectral functions were obtained in terms of the *defect wave functions* and the binding energy of two protons in the ^{16}O nucleus in the limited harmonic oscillator shell-model

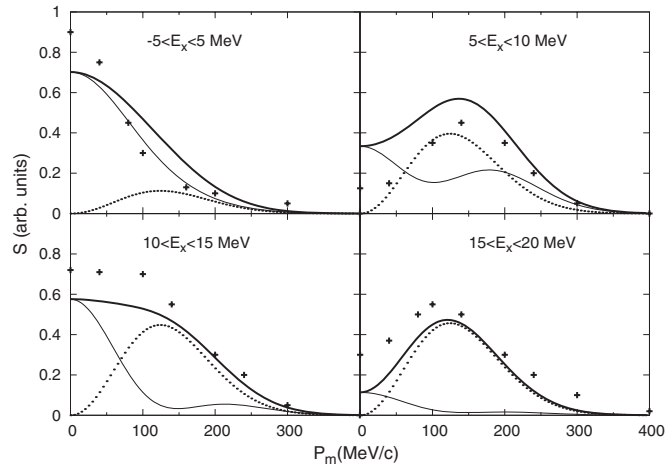

FIG. 11. Measured ^{16}O$(e, e' pp)^{14}$C cross section (TNSF) in terms of missing momentum and different range of excitation energies. The full curves are ${}^1S_0$, the dash curves are ${}^3P_J$, the heavy full curves are the total, and the pluses are the sum of all channels from the experimental data [8].

space. Both the long- and short-range correlations for the calculation of two-proton-removal spectral functions were taken into account. It was shown that the defect functions for all channels are important (ignorable) for low (high) relative momenta, $p < 4$ fm^{-1} ($p > 4$ fm^{-1}). The LOCV TNSF were compared both with the theoretical (DRPA) calculation and the experimental data (Onderwater *et al.*). It was shown that $^1S_0$ proton-pair emission in the ^{16}O$(e, e'pp)^{14}$C reaction is dominant with respect to the other proton-pair relative states. It was also demonstrated that the 0^+ and the 2^+ peaks, which were expected to be observed in the the above reaction cross section, moved to lower momentum of out-going protons, when the state-dependent correlation functions were imposed. In this work we ignored the center-of-mass dependence of our state-dependent correlations. We hope in our future work that this dependence can be taken into account.

ACKNOWLEDGMENTS

We would like to thank the Research Council of University of Tehran and Institute for Research and Planning in Higher Education for the grants provided us.

[1] W. J. W. Geurts, K. Allaart, W. H. Dickhoff, and H. Müther, Phys. Rev. C **54**, 1144 (1996).
[2] W. J. W Geurts, Ph.D. thesis, Vrije Universiteit, 1996.
[3] C. Giusti, F. D. Pacati, K. Allaart, W. J. W. Geurts, W. H. Dickhoff, and H. Müther, Phys. Rev. C **57**, 1691 (1998).
[4] C. Barbieri, C. Giusti, F. D. Pacati, and W. H. Dickhoff, Phys. Rev. C **70**, 014606 (2004).
[5] O. Benhar and A. Fabrocini, Phys. Rev. C **62**, 034304 (2000).
[6] C. Ciofi degli Atti and S. Simula, Phys. Rev. C **53**, 1689 (1996).
[7] H. Müther and A. Polls, Prog. Part. Nucl. Phys. **45**, 243 (2000).
[8] C. J. G. Onderwater *et al.*, Phys. Rev. Lett. **78**, 4893 (1997).
[9] C. Giusti and F. D. Pacati, Nucl. Phys. A **535**, 573 (1991).
[10] C. Giusti, F. D. Pacati, and M. Radici, Nucl. Phys. A **546**, 607 (1992).
[11] C. Giusti and F. D. Pacati, Nucl. Phys. A **571**, 694 (1994).
[12] C. Giusti and F. D. Pacati, Nucl. Phys. A **585**, 618 (1995).
[13] C. Giusti and F. D. Pacati, Nucl. Phys. A **641**, 297 (1998).
[14] C. J. G. Onderwater *et al.*, Phys. Rev. Lett. **81**, 2213 (1998).
[15] R. Starink *et al.*, Phys. Lett. B **474**, 33 (2000).
[16] J. C. Owen, R. F. Bishop, and J. M. Irvine, Phys. Lett. B **59**, 1 (1975).
[17] J. C. Owen, R. F. Bishop, and J. M. Irvine, Ann. Phys. (NY) **102**, 170 (1976).
[18] J. C. Owen, R. F. Bishop, and J. M. Irvine, Nucl. Phys. A **274**, 108 (1977).
[19] M. Modarres and J. M. Irvine, J. Phys. G: Nucl. Part. Phys. **5**, 511 (1979).
[20] M. Modarres and G. H. Bordbar, Phys. Rev. C **58**, 2781 (1998).
[21] G. H. Bordbar and M. Modarres, Phys. Rev. C **57**, 714 (1998).
[22] M. Modarres, A. Rajabi, and H. R. Moshfegh, Phys. Rev. C **76**, 064311 (2007).
[23] M. Modarres and N. Rasekhinejad, Phys. Rev. C **72**, 014301 (2005).
[24] M. Modarres and N. Rasekhinejad, Phys. Rev. C **72**, 064306 (2005).
[25] M. Modarres and Y. Younesizadeh, Nucl. Phys. A **789**, 82 (2007).
[26] M. Modarres and Y. Younesizadeh, Int. J. Theor. Phys. **49**, 413 (2010).
[27] M. Modarres and Y. Younesizadeh, Int. J. Mod. Phys. E **20**, 2209 (2011).
[28] R. V. Reid, Ann. Phys. (NY) **50**, 411 (1968).
[29] R. B. Wiringa, V. G. J. Stoks, and R. Schiavilla, Phys. Rev. C **51**, 38 (1995).
[30] A. L. Fetter and J. D. Walecka, *Quantum Theory of Many-Particle Physics* (McGraw-Hill, New York, 1971).
[31] A. R. Edmonds, *Angular Momentum in Quantum Mechanics* (Princeton University Press, Princeton, 1957).
[32] P. J. Brussaard and P. W. M. Glaudemans, *Shell-Model Applications in Nuclear Spectroscopy* (North-Holland, Amsterdam, 1977).
[33] J. W. Clark and E. Feenberg, Phys. Rev. **113**, 388 (1959).
[34] J. W. Clark, Prog. Part. Nucl. Phys. **2**, 89 (1979).
[35] R. Jastrow, Phys. Rev. **98**, 1479 (1955).
[36] M. Modarres and H. R. Moshfegh, Prog. Theor. Phys. **112**, 21 (2003).
[37] M. Modarres, N. Rasekhinejad, and H. Mariji, Int. J. Mod. Phys. E **20**, 679 (2011).
[38] M. Modarres, M. Mariji, and N. Rasekhinejad, Nucl. Phys. A **859**, 16 (2011).
[39] T. Brody and M. Moshinsky, *Tables of Transformation Brackets* (Mexico Instituto de Fisica, 1960).
[40] V. R. Pandharipande and R. B. Wiringa, Rev. Mod. Phys. **51**, 821 (1979).
[41] C. Giusti and F. D. Pacati, Nucl. Phys. A **615**, 373 (1997).
[42] S. C. Pieper, R. B. Wiringa, and V. R. Pandharipande, Phys. Rev. C **46**, 1741 (1992).
[43] S. Fantoni and V. R. Pandharipande, Phys. Rev. C **37**, 1697 (1988).
[44] H. Müther and P. U. Sauer, in *Computational Nuclear Physics*, edited by K.-H. Langanke, J. A. Maruhn, and S. E. Koonin (Springer, New York, 1993).
[45] F. Ajzenberg-S, Nucl. Phys. A **523**, 1 (1991).
[46] F. Ajzenberg-S, Nucl. Phys. A **460**, 1 (1986).
[47] L. J. H. M. Kester, Ph.D. thesis, NIKHEF, 1993.
[48] W. H. A. Hesselink and E. Jans, NIKHEF-K proposal NR:94-1.